Investigation of the porous nanostructured Cu/Ni/AuNi electrode for sodium borohydride electrooxidation

ARTICLE *in* ELECTROCHIMICA ACTA · DECEMBER 2013

Impact Factor: 4.5 · DOI: 10.1016/j.electacta.2013.10.012

3 AUTHORS:

Mir ghasem Hosseini
University of Tabriz
118 PUBLICATIONS **1,814** CITATIONS
SEE PROFILE

Mehdi Abdolmaleki
Sayyed Jamaleddin Asadabadi University
16 PUBLICATIONS **73** CITATIONS
SEE PROFILE

Farzad Nasirpouri
Sahand University of Technology
59 PUBLICATIONS **260** CITATIONS
SEE PROFILE

Electrochimica Acta 114 (2013) 215–222

Contents lists available at ScienceDirect

Electrochimica Acta

journal homepage: www.elsevier.com/locate/electacta

Investigation of the porous nanostructured Cu/Ni/AuNi electrode for sodium borohydride electrooxidation

Mir Ghasem Hosseini [a,*], Mehdi Abdolmaleki [a], Farzad Nasirpouri [b]

[a] Electrochemistry Research Laboratory, Department of Physical Chemistry, Chemistry Faculty, University of Tabriz, Tabriz 0098 5166616471, Iran
[b] Department of Materials Engineering, Sahand University of Technology, Tabriz, Iran

ARTICLE INFO

Article history:
Received 16 July 2013
Received in revised form
28 September 2013
Accepted 3 October 2013
Available online 18 October 2013

Keywords:
Borohydride electrooxidation
Electrocatalyst
Galvanic replacement
Cyclic voltammetry
Direct borohydride fuel cell
Electrochemical impedance spectroscopy

ABSTRACT

An electrochemical approach to nanostructured Cu/Ni/AuNi catalyst design using the electrodeposition process followed by galvanic replacement technique is presented. The procedure consisted of the electrodeposition of Ni–Zn on the Ni coating with subsequent replacement of the zinc by gold at open circuit potential in a gold containing alkaline solution. The surface morphologies and compositions of coatings were determined by energy dispersive X-ray and scanning electron microscopy techniques. The results showed that the Cu/Ni/AuNi coatings were porous composing of discrete Au nanoparticles. The electrocatalytic activity of Cu/Ni/AuNi electrodes for sodium borohydride electro-oxidation was studied using cyclic voltammetry, chronoamperometry, chronopotentiometry and electrochemical impedance spectroscopy techniques. The electro-oxidation current on Cu/Ni/AuNi catalyst is much higher than that on flat Au catalyst. The onset potential and peak potential on Cu/Ni/AuNi catalysts are more negative than that on flat Au catalyst for borohydride electrooxidation. The impedance behavior also shows different patterns, capacitive, and negative resistances and inductive loops at different applied anodic potentials. All results show that the Cu/Ni/AuNi catalysts can be applied as potential anode catalysts for the direct borohydride fuel cells.

1. Introduction

The increasing demand for efficient and clean power sources has greatly stimulated the research and development of low-temperature fuel cells for stationary and mobile applications [1,2]. Several promising fuels, e.g. hydrogen and methanol, have been intensively evaluated and concerns in poisoning, supply and storage, capacity and efficiency, toxicity were raised [1–4]. In recent years, aqueous solution of sodium borohydride has been widely studied as fuel in direct borohydride fuel cell (DBFC). The fuel (borohydride salt), also presents several advantages: it is non-toxic, can easily be stored and relatively stable in alkaline solution, while exhibits rather high energy density (9.3 Wh g^{-1} at 1.64 V) [5–8]. Borohydride fuel cells are currently under active investigation as part of worldwide efforts to develop environmentally sustainable sources of power [7–12].

The oxidation reaction of borohydride can take place with an eight-electron process described as follows (Eq. (1)) [13]:

$$BH_4^- + 8OH^- \rightarrow BO_2^- + 6H_2O + 8e^- \quad E^0 = -1.24\,\text{Vvs.SHE} \qquad (1)$$

However, this reaction is barely found to happen in practice because the anodic reactions on the electrodes have to compete with the hydrolysis reaction. The hydrolysis of borohydride ion produces hydrogen gas and a number of borohydroxide or oxide intermediates that deplete the amount of borohydride ions available for oxidation (Eq. (2)) [14,15].

$$BH_4^- + yH_2O \rightarrow BH_{4-y}^-(OH)_y + yH_2 \quad (y = 1\text{–}4) \qquad (2)$$

The electrochemical reaction of borohydride depends on the catalysts material, alkaline solution concentration and also on temperature.

Pt- or Au-based binary electrocatalysts tested in reactions relevant to fuel cell technology (oxygen reduction [16,17]; methanol oxidation [18,19]; borohydride oxidation [20]) constitute a large part of recent electrochemical literature.

The galvanic replacement procedure provides a very simple and effective method to prepare porous bimetallic nanostructures having a lower standard electrode potential compared to that of the target material.

In this work, we demonstrate a procedure for synthesizing porous Cu/Ni/AuNi nanostructures via galvanic exchange reaction using Zn from Cu/Ni/ZnNi coating. NiZn coating was grown on Ni by electrodeposition technique and Cu/Ni/ZnNi electrode was obtained. Porous Cu/Ni/AuNi nanostructures were produced by exposing the Cu/Ni/ZnNi electrode to an alkaline aqueous solution

* Corresponding author. Tel.: +98 4113393138; fax: +98 4113340191.
E-mail address: mg-hosseini@tabrizu.ac.ir (M.G. Hosseini).

0013-4686/$ – see front matter © 2013 Elsevier Ltd. All rights reserved.
http://dx.doi.org/10.1016/j.electacta.2013.10.012

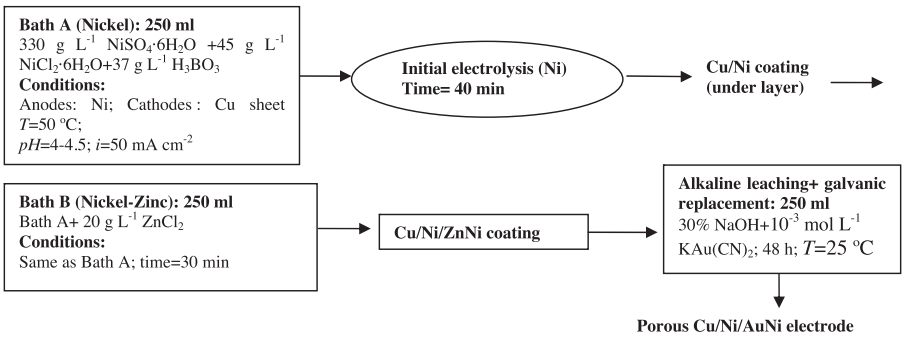

Fig. 1. Flowchart of typical preparation procedure for the nanostructured Cu/Ni/AuNi electrodes.

of the corresponding gold salt (10^{-3} mol L^{-1} $KAu(CN)_2$ + 30 wt.% NaOH). These porous nanostructures are stable under ambient conditions and show a highly porous catalytic surface suitable for the electrooxidation of borohydride in alkaline solution.

2. Experimental

All reagents used in this work were of analytical grade provided by Merck were used without further purification. All solutions were prepared using double distilled water. The Cu/Ni/AuNi catalysts were prepared through the electrodeposition and galvanic replacement processes. A typical preparation procedure for the nanostructured Cu/Ni/AuNi electrode is presented in Fig. 1. In detail, the copper substrates (cathodes) were cut and mounted in polyester resin except a surface area of 1 cm^2 for measurements. Electrical conductivity was provided by soldering a copper wire. Before electrodeposition, the electrode surfaces were polished with emery paper (2500 grit size), then washed with double distilled water, thoroughly degreased in a 30 wt.% NaOH solution for 5 min, washed again with distilled water, dipped into 10 wt.% H_2SO_4 solution for 1 min followed by a rinse with distilled water and immersed in the bath solution. The plating baths and conditions used for the smooth Ni and Cu/Ni/ZnNi coatings are given in Fig. 1. After deposition, the electrodes were rinsed with distilled water in order to remove residues of bath chemicals and unattached particles. The Au deposition was performed simply by immersing the Cu/Ni/ZnNi electrode into a 30 wt.% NaOH solution of $KAu(CN)_2$ salt (Merck, 99.99%) with concentration of 10^{-3} mol L^{-1} for 48 h at room temperature.

The standard reduction potential of the Au^+/Au pair (1.691 V vs. SHE) is higher than reduction potential of the Zn^{+2}/Zn pair (−0.762 V vs. SHE), and it can be reduced by Zn as shown in the following equation:

$$Zn + 2Au(CN)_2^- \rightarrow 2Au + Zn^{+2} + 4CN^- \quad (3)$$

Finally, the electrode was removed from the solution and washed with double distilled water thoroughly. The surface composition and morphology of electrodes before and after galvanic replacement were determined using scanning electron microscopy (SEM, Philips, and Model XL30) equipped with an energy dispersive X-ray (EDX) spectrometer.

The electrochemical studies were carried out in a conventional three-electrode electrochemical cell and all the solutions were purged with purified nitrogen for 10 min before the measurements. A platinum sheet of the geometric area of about 20 cm^2 was used as counter electrode, while all potentials were measured with respect to a commercial saturated calomel electrode (SCE). Cyclic voltammetry (CV), chronoamperometry, chronopotentiometry and electrochemical impedance spectroscopy (EIS) experiments were performed using a Princeton Applied Research, EG&G PARSTAT 2263 Advanced Electrochemical system run by PowerSuite software.

The impedance spectra were recorded in a frequency range of 100 kHz to 10 mHz, with the amplitude (r.m.s. value) of the ac signal being 10 mV. The acquired data were curve fitted and analyzed using ZView(II) software.

3. Results and discussion

3.1. Characterization of coatings

The SEM images of Cu/Ni/ZnNi electrode and Cu/Ni/AuNi electrode are given in Fig. 2. It can be seen from Fig. 2a that the surface

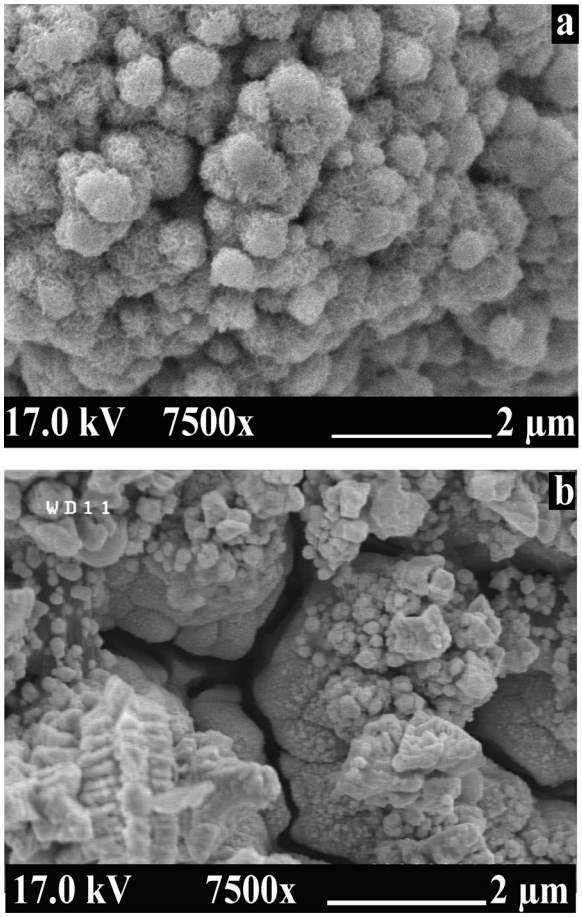

Fig. 2. SEM images of (a) Cu/Ni/ZnNi coating and (b) Cu/Ni/AuNi coating after leaching-galvanic replacement process.

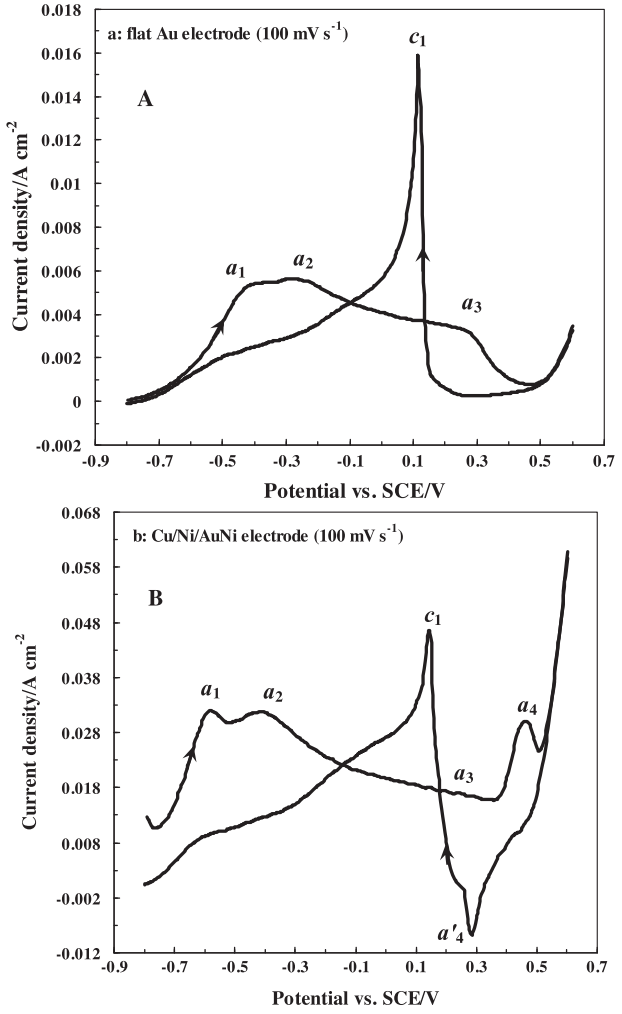

Fig. 3. Cyclic voltammograms of flat Au electrode (a) and porous Cu/Ni/AuNi electrode (b) in a solution containing 2 M NaOH and 0.02 M sodium borohydride at a potential sweep rate of 100 mV s^{-1}.

of Ni was fully covered by the NiZn layer. The Cu/Ni/ZnNi coating is compact and has a porous structure. However, the morphology of surface changed significantly after leaching-galvanic replacement process of Zn from the deposit (Fig. 2b). A great number of cracks and pores appeared leading a high surface area available for the borohydride oxidation reaction. Cu/Ni/AuNi deposits are nano-particulate and retain a high coverage of the substrate.

The EDX analysis showed that the chemical composition of surface before leaching-replacement was 16.87 at.% Ni and 83.13 at.% Zn. After alkaline leaching-galvanic replacement, the surface composition was changed as 59.47 at.% Ni, 28.28 at.% Zn and 12.25 at.% Au. The results of chemical composition analysis revealed that the Zn content decreased considerably after selective dissolution, which leads to pore and crack formation, yielding a highly porous surface suitable for use in borohydride electrooxidation. Also, EDX results confirm the presence of gold nanoparticles on the surface film.

3.2. Cyclic voltammetry

Fig. 3 shows the cyclic voltammetry of 2 M NaOH + 0.02 M $NaBH_4$ solution on porous Cu/Ni/AuNi and flat Au electrodes with the same geometric area (1 cm^2). The potential was swept between −0.8 and 0.6 V at 100 mV s^{-1} during the experiments. The BH_4^- CV at a flat gold electrode is characterized by four oxidation peaks (Fig. 3A). Peaks of a_1 and a_2 are seen as a wide oxidation wave can be identified between −0.6 and −0.1 V versus SCE. This wave is consistent with previously reported BH_4^- voltammograms obtained on a flat Au surface due to the overall eight-electron oxidation of BH_4^- (Eq. (1)) [21–24].

Then, a broad oxidation hump (that develops into a broad shoulder peak a_3) appears, which can be attributed to the oxidation of reaction intermediates on the partially oxidized gold surface. The sharp peak that is observed in the reverse direction (c_1) is thought to be due to the oxidation of adsorbed BH_3OH^- that is formed in the BH_4^- chemical hydrolysis (Eq. (2)) [24]. The borohydride electro-oxidation on Cu/Ni/AuNi electrode was characterized by six well-defined current peaks on the forward and reverse scans (Fig. 3B). An increment in the anodic peak current for previous peaks (a_1, a_2, a_3 and C_1) followed by the appearance of two new peaks (a_4 and a'_4) at more positive potential are the main effects observed upon electro-oxidation of borohydride on the porous Cu/Ni/AuNi electrode. Peak a_1 could be due to the oxidation of H_2 generated in the catalytic hydrolysis of $NaBH_4$. Because, on the vast majority of metals and alloys studied in relation to BH_4^- oxidation (e.g., Ni, Pt, Pd, Ni_xB) the complete eight-electron exchange is not achieved. Furthermore, on metals leading to the incomplete oxidation of borohydride the Faradaic reaction is typically accompanied by the catalytic hydrolysis of BH_4^- yielding H_2 and a number of potential borohydroxide (or oxide) intermediates (Eq. (2)) [14,15]. The second anodic oxidation occurring at −0.4 V (peak a_2) is related to the direct oxidation of BH_4^- through a reaction mechanism involving eight electrons [23,25]. The new peaks (a_4 and a'_4) can be attributed to the interconversion of $Ni(OH)_2$ and NiOOH in alkaline media [26]. Also, the peak a_3 is not seen. The appearance of the new peaks leads to the conclusion that borohydride oxidation takes place after the oxidation of $Ni(OH)_2$ to NiOOH [27–30]. The Ni^{2+}/Ni^{3+} redox couple acts as a catalyst for the oxidation of borohydride in basic solutions.

According to Aytaç et al. [31], electrochemical oxidation of $NaBH_4$ at Ni electrodes is represented by

$$Ni + 2OH^- \rightarrow Ni(OH)_2 + 2e^- \quad (4)$$

$$Ni(OH)_2 + OH^- \rightarrow NiOOH + H_2O + e^- \quad (5)$$

$$8NiOOH + NaBH_4 + 2H_2O \rightarrow 8Ni(OH)_2 + NaBO_2 \quad (6)$$

The active NiOOH formed during the positive potential scan is consumed through reaction (6). Subsequently, the formed $Ni(OH)_2$ in reaction (6) is again oxidized to NiOOH during the anodic potential sweep. This results in an increase in oxidation currents in the presence of $NaBH_4$.

As shown in Fig. 3, the current density of the Cu/Ni/AuNi electrode is much higher than flat Au electrode. For example, at the potential of peak a_2, the Cu/Ni/AuNi electrode presents a current density of about 31 mA cm^{-2}, nearly six times higher than that of the flat Au electrode (5.2 mA cm^{-2}). Also, the onset potential of the borohydride electro-oxidation reaction on porous Cu/Ni/AuNi electrode (−0.475 V vs. SCE) is more negative than flat Au electrode (−0.35 V vs. SCE). These results confirm that the leaching-galvanic replacement method can provide a high electrochemically active area for use in borohydride electrooxidation.

The influence of the potential scan rate on the cyclic voltammetry behavior of porous Cu/Ni/AuNi nano structured electrode in 2 M NaOH/0.02 M borohydride solution is shown in Fig. 4A. The a_2 peak current density (I_{pa2}) has shown a linear increase with the square root of the scan rate, indicating diffusion-controlled electrocatalytic oxidation (Fig. 4B). The a_2 peak potential (E_{p2}) also linearly changed with the logarithm of the scan rate showing that an irreversible electrode reaction takes place on the Cu/Ni/AuNi electrode surface (Fig. 4C).

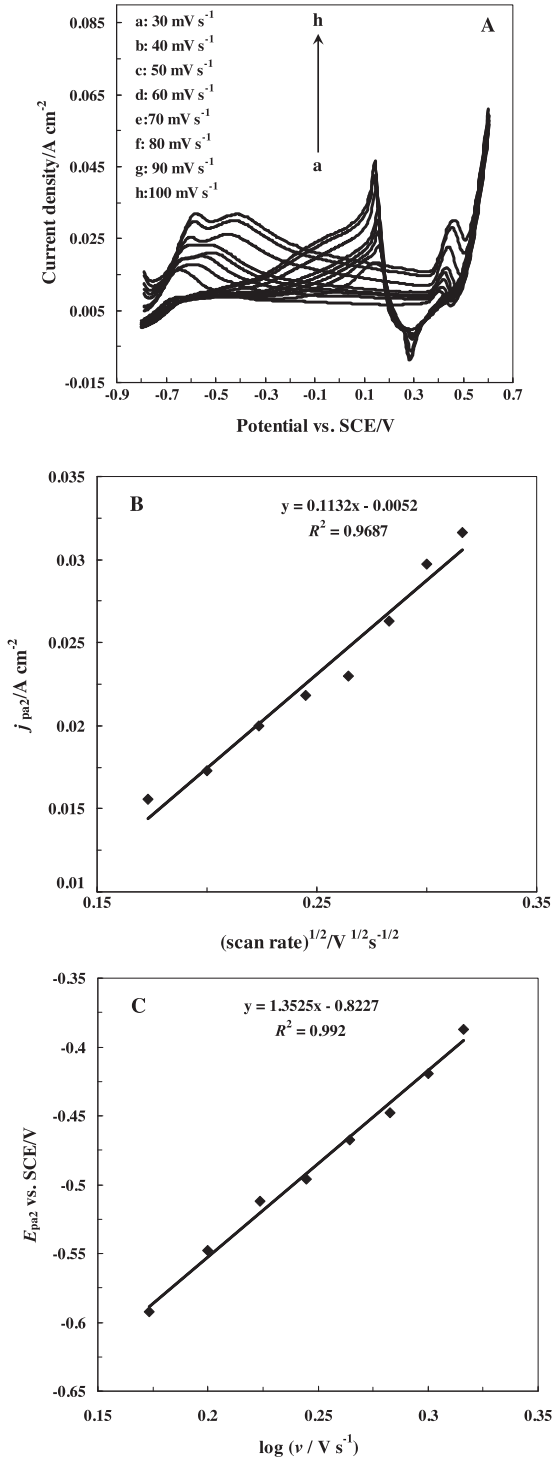

Fig. 4. (A) The cyclic voltammograms for porous Cu/Ni/AuNi electrode in 2 M NaOH + 0.02 M $NaBH_4$ at different scan rate. (B) The plot of borohydride oxidation peak current on the porous Cu/Ni/AuNi electrode versus (scan rate)$^{1/2}$. (C) The plot of variation of peak potential with logarithm of the scan rate for the porous Cu/Ni/AuNi electrode.

The total number of electrons (n) can be determined using the following equation [32–34]:

$$I_{pa} = 2.99 \times 10^5[(1-\alpha)n_a]^{1/2} n A C_0 (D_0 \nu)^{1/2} \quad (7)$$

where I_{pa} is the peak current (A) in CV, A is the geometric electrode area (cm^2), D_0 is the diffusion coefficient ($cm^2\ s^{-1}$), n_a is the number of electrons involved in the rate determining step (being 1 the most likely value), C_0 is the bulk borohydride concentration ($mol\ cm^{-3}$), ν is the potential sweep rate ($V\ s^{-1}$) and α is the charge transfer coefficient for the oxidation step, which can be determined by the linear dependence of peak potential E_{Pa} with the logarithm of the potential scan rate ν (Fig. 4C), according to [32–34]:

$$E_{pa} = E^0 + \left\{\frac{2.3RT}{(1-\alpha)n_aF}\right\} \times \left\{0.52 - \frac{1}{2}\log\left[\frac{2.3RT}{(1-\alpha)n_aFD_0}\right] - \log k_s + \frac{1}{2}\log\nu\right\} \quad (8)$$

where E_{pa} is the peak potential (V vs. SCE), E^0 is the formal potential (V vs. SCE), R is the universal gas constant ($8.314\ J\ K^{-1}\ mol^{-1}$), T is the temperature (K), F is the Faraday constant ($96{,}485\ C\ mol^{-1}$) and k_s is the standard heterogeneous rate constant ($cm\ s^{-1}$).

From Eqs. (7) and (8) and the slopes extracted from Fig. 4B and C, the values of the $nD_0^{1/2}$ relation and α were calculated as being $0.01338\ cm\ s^{-1/2}$ and 0.98, respectively. As expected, the calculated α value ($\alpha = 0.98$) confirms a highly irreversible process related to the a_2 peak. If diffusion coefficient is estimated at $1.0 \times 10^{-5}\ cm^2\ s^{-1}$ using the Stokes–Einstein equation [35,36], the value of n was calculated as 4.23

Fig. 5 shows the typical CVs for Cu/Ni/AuNi electrode as a function of $NaBH_4$ concentration between 0.02 and 0.07 M. The a_2

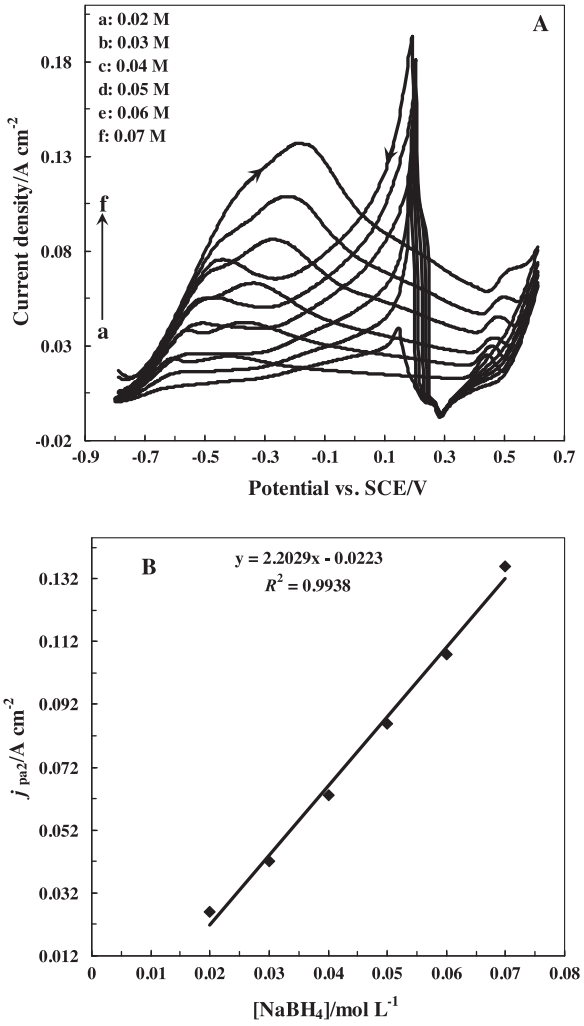

Fig. 5. (A) Cyclic voltammograms of the porous Cu/Ni/AuNi electrode from −0.8 to 0.6 V at the scan rate of $100\ mV\ s^{-1}$ with the various concentrations of borohydride. (B) The plot of borohydride oxidation peak current on the porous Cu/Ni/AuNi electrode versus concentration of borohydride.

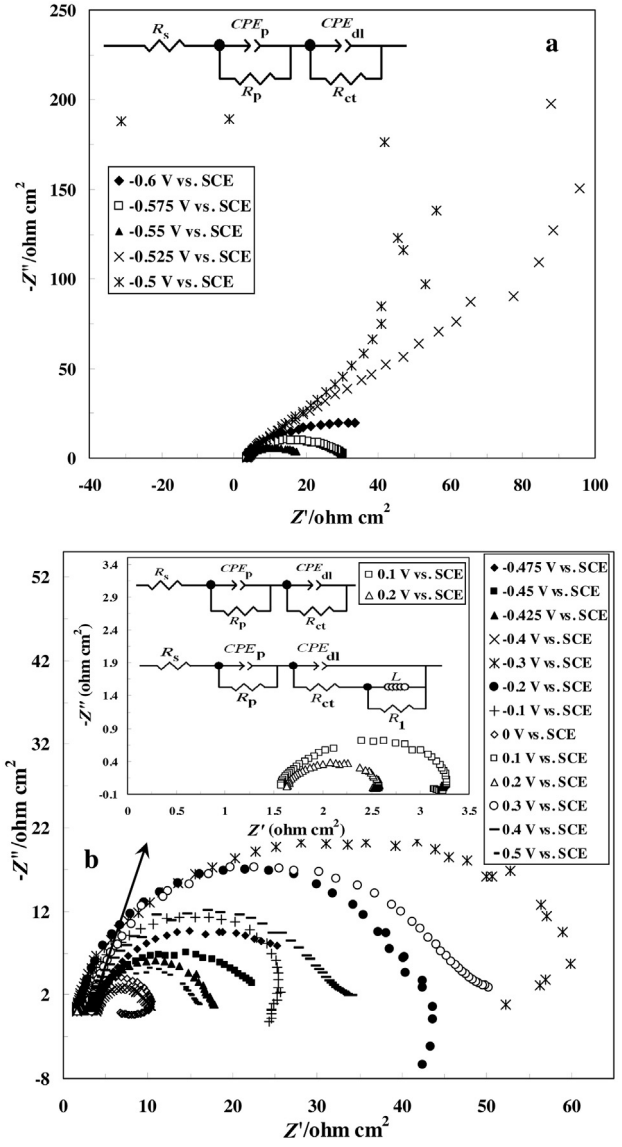

Fig. 6. Experimental Nyquist diagrams and equivalent electrical circuits for borohydride electro-oxidation at the Cu/Ni/AuNi electrode in 2 M NaOH + 0.02 M borohydride aqueous solutions in varied potential regimes: (a) in the potential between −0.6 and −0.5 V vs. SCE and (b) in the potential between −0.475 and 0.5 V vs. SCE.

peak potential shifted slightly toward more positive values with increasing $NaBH_4$ concentration. The corresponding peak current density increased linearly with increasing concentration, as shown by Fig. 5B. The linear dependence of I_{pa} upon the borohydride concentrations allows us to suggest that the Cu/Ni/AuNi electrode could conveniently be used in the electroanalytical determination of sodium borohydride.

3.3. EIS results

The Nyquist plots and equivalent electrical circuits of the impedance of the Cu/Ni/AuNi electrode for borohydride electro-oxidation at different potentials in 2 M NaOH/0.02 M borohydride solution are shown in Fig. 6. Nyquist plots of presented in Fig. 6 suggest porosity of the electrode surfaces. Typically, Nyquist plots of porous electrodes show either a line with a slope of 45° or a semicircle at high frequencies followed by a semicircle at low frequencies [37,38]. The impedance data of electro-oxidation of $NaBH_4$ at Cu/Ni/AuNi electrodes were fitted using the equivalent circuits shown in the inset of the Nyquist diagrams in Fig. 6. Symbols, R_s, R_P, R_{ct}, and R_1 represent the solution, pore, charge transfer and adsorption resistances, respectively; CPE_p and CPE_{dl} represent the constant phase elements (CPE) for the porous electrode and the catalyst/solution interface, respectively; and L represents an inductance which is used to account for the impedance contribution of the adsorption and desorption processes taking place at the composite electrode at low frequencies [39,40].

The CPE is defined by two parameters, T and Φ, in the equation for impedance [41]:

$$Z_{CPE} = \frac{1}{T(j\omega)\phi} \quad (9)$$

where Z_{CPE} is constant phase element impedance, T is the admittance factor, Φ is the phase shift which can be explained as a degree of surface homogeneity. The EIS results indicate that the borohydride electro-oxidation on the nanostructured Cu/Ni/AuNi catalyst at various potentials shows different impedance behaviors.

As it can be clearly seen from Fig. 6a, with the increase of anodic potentials, the diameter of arc decreases rapidly, indicating that the charge transfer resistance for the H_2 electro-oxidation becomes smaller. The main reason is that the first oxidation peak occurs at −0.55 V (peak a_1) was due to the oxidation of H_2 generated during catalytic hydrolysis of $NaBH_4$. As potentials arrive at −0.525 V, a sudden change of impedance plots happens, with the loop reversing to the 2nd quadrant as shown in Fig. 6a. The main reason is that the electrochemical reaction changes from the oxidation of H_2 to the direct oxidation of BH_4^- as substantiated by CV results, which leads to the reversal of impedance to the second quadrant.

It is observed from Fig. 6b that the charge transfer resistance decreased with increasing potential because borohydride electro-oxidation reaction commences at potentials higher than −0.5 V. In the potential between −0.3 and 0.2 V (Fig. 6b), a so-called 'pseudo-inductive' behavior begins to emerge in the impedance plots, where two large positive loop at higher frequency is accompanied by a small loop in the fourth quadrant at low frequency, with both diameters of the loops decreasing rapidly with the increase of the potential between −0.3 and 0.2 V as shown in Fig. 6b. An explanation for the occurrence of inductive behavior during borohydride electro-oxidation can be the oxidation of reaction intermediates (such as BH_3OH^-) during the oxidation of BH_4^- on gold electrode and creation of sites for possible adsorption and further reaction [24]. In the potentials between 0.3 and 0.5 V (Fig. 6b), the diameters of large semicircles decrease sharply with increasing potential. This result confirms the formation of $Ni(OH)_2$/NiOOH couple as a catalyst for the oxidation of borohydride in basic solutions at higher anodic potential [27–30]. These observations are consistent with the results of CVs.

Table 1 shows the values of the equivalent circuit elements obtained by fitting the experimental results. Also the mean error of modulus is smaller than 6%, indicating a good fitting of the experimental data on the developed equivalent circuit.

In order to electrochemically characterize the real surface of the Cu/Ni/AuNi electrode with flat Au electrode, the surface area of the electrodes was determined by recording the impedance plots at the borohydride electro-oxidation reaction onset potentials. Fig. 7 presents the equivalent circuits and Nyquist diagrams of flat Au and porous Cu/Ni/AuNi electrodes recorded at anodic onset potential of sodium borohydride electro-oxidation, both in 2 M NaOH/0.02 M borohydride solution. For the Cu/Ni/AuNi electrode,

Table 1
Equivalent circuit parameters of electro-oxidation of 0.02 M borohydride on the porous Cu/Ni/AuNi electrode in 2 M NaOH solution obtained from Fig. 6.

E (V) vs. SCE	R_s (ohm cm^2)	T_P (ohm^{-1} cm^{-2} s$^{\Phi}$)	R_P (ohm cm^2)	Φ_p	T_{dl} (ohm^{-1} cm^{-2} s$^{\Phi}$)	R_{ct} (ohm cm^2)	Φ_{dl}	L (H)	R_1 (ohm cm^2)	Error (%)
−0.6	3.684	0.0003319	25.23	0.86	0.0009694	33.67	0.90	–	–	2.07
−0.575	3.634	0.01123	4.353	0.83	0.000357	22.99	0.87	–	–	2.07
−0.55	3.7	0.005225	4.59	0.92	0.0002268	12.92	0.88	–	–	2.22
−0.525	3.5	0.0015371	53.14	0.76	0.0025375	−1499	0.76	–	–	2.34
−0.5	3.47	0.0039279	54.28	0.69	0.0031756	−300.1	0.76	–	–	3.8
−0.475	3.7	0.002547	8.998	0.94	0.0006317	20.31	0.83	–	–	2.18
−0.45	3.65	0.0004028	9.904	0.89	0.001679	10.02	0.87	–	–	2.09
−0.425	3.71	0.07037	3.475	0.92	0.0001631	8.82	1	–	–	2.07
−0.4	3.95	0.06235	0.791	0.78	0.0003084	6.02	0.94	–	–	1.48
−0.3	1.56	0.0012254	18.1	0.89	0.0031376	38.51	0.85	12.81	3.015	3.9
−0.2	1.547	0.0062149	13.69	0.99	0.033583	29.3	0.75	524.2	15.03	1.25
−0.1	1.56	0.011558	0.244	0.92	0.0059726	23.32	0.86	4.6	3.302	5.5
0.0	1.573	0.0028338	0.13	0.76	0.0056171	6.078	0.89	5.335	2.715	1.25
0.1	1.581	0.003004	0.277	1	0.0048508	1.3	0.95	0.204	0.13	1.5
0.2	1.65	0.001703	0.3112	1	0.0053345	0.566	0.97	0.0119	0.0446	1.6
0.3	3.267	0.008793	11.34	0.80	0.0003398	35.11	0.92	–	–	2.23
0.4	3.266	0.0386	4.66	0.77	0.0003659	26.55	0.91	–	–	2.22
0.5	3.275	0.01273	2.425	0.82	0.0004468	10.2	0.93	–	–	2.07

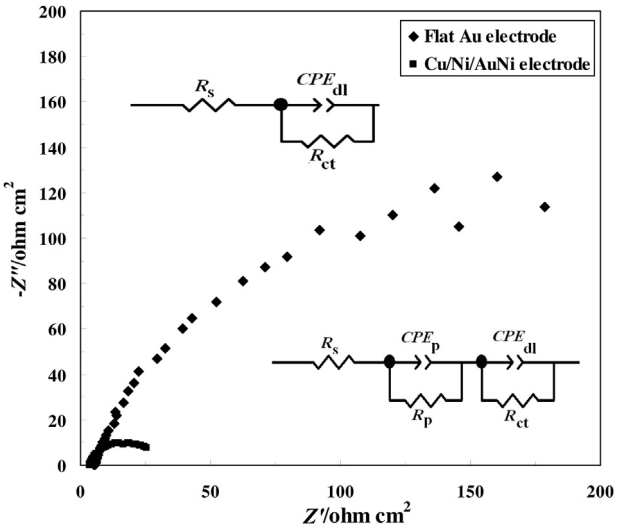

Fig. 7. Equivalent circuits and Nyquist diagrams at the borohydride electro-oxidation onset potentials of flat Au (−0.35 V vs. SCE) and porous Cu/Ni/AuNi (−0.475 V vs. SCE) electrodes in 2 M NaOH + 0.02 M borohydride solution.

the capacitance parameter T_{dl} is related to the average double layer capacitance C_{dl} by the relation [40]:

$$C_{dl} = \left\{ \frac{T_{dl}}{[(R_s + R_p)^{-1} + R_{ct}^{-1}]^{(1-\phi)}} \right\}^{1/\phi}, \quad (10)$$

while in the case of flat Au electrode, the capacitance parameter T_{dl} is also related to the average double layer capacitance C_{dl} by a slightly different relation [40]:

$$(11) C_{dl} = \left\{ \frac{T_{dl}}{[R_s^{-1} + R_{ct}^{-1}]^{(1-\phi)}} \right\}^{1/\phi}$$ because the corresponding Nyquist diagram exhibits only one semicircle. The model of the equivalent circuit includes the constant phase element (CPE) in parallel with the charge transfer resistance R_{ct} (shown in the inset of the Nyquist diagram in Fig. 7). Taking that the average double layer capacitance (C_{dl}) of a smooth metal surface is 20 μF cm^{-2} [42,43], real surface area for the electrodes can be calculated as $A_{real} = C_{dl}/20$ (cm^2), and then the roughness factor, that characterizes the real-to-geometrical surface area ratio, can be calculated from $R_f = A_{real}/A_{geometric}$.

The mean values of the charge transfer resistance, double layer capacitance, true surface, and roughness factor for the investigated electrodes are presented in Table 2. As it can be seen from Table 2, the surface area of Cu/Ni/AuNi electrode was found to be 10.644 cm^2 while the flat Au electrode gives a smaller real surface area of 5.198 cm^2.

Table 2
Parameters obtained by fitting EIS results of Fig. 7.

Element	Flat Au electrode	Cu/Ni/AuNi electrode
R_s (ohm cm^2)	5.22	3.7
T_P (ohm^{-1} cm^{-2} s$^{\Phi}$)	–	0.002547
R_P (ohm cm^2)	–	8.998
Φ_p	–	0.94
T_{dl} (ohm^{-1} cm^{-2} s$^{\Phi}$)	0.0002382	0.0006317
R_{ct} (ohm cm$^{2)}$	301.9	20.31
Φ_{dl}	0.89	0.83
C_{dl} (μF cm^{-2})	103.97	212.88
A_{real} (cm^2)	5.198	10.644
R_f	5.198	10.644
Error (%)	3.82	2.18

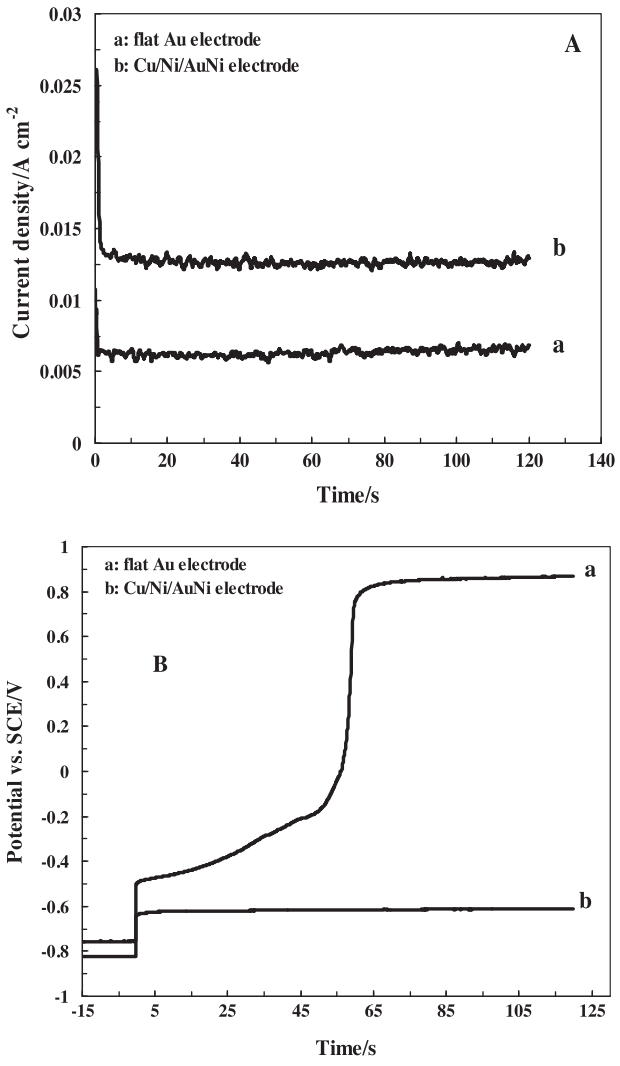

Fig. 8. (A) Chronoamperometry curves of flat Au and Cu/Ni/AuNi electrodes in 2 M NaOH + 0.02 M $NaBH_4$ solution. Potential step: from −0.8 to −0.1 V vs. SCE. (B) Chronopotentiometry curves of flat Au and Cu/Ni/AuNi electrodes in 2 M NaOH + 0.02 M $NaBH_4$ solution. Current step: from 0 to 5 mA cm^{-2}.

Also, the lowest R_{ct}, 20.31 ohm cm^2, was observed on porous Cu/Ni/AuNi electrode. This means that the catalytic activity of Cu/Ni/AuNi electrode is higher than that of the flat Au electrode. According to cyclic voltammograms depicted in Fig. 3, the novel Cu/Ni/AuNi electrode produced about six times higher anodic current density compared to that on flat Au electrode in 2 M NaOH + 0.02 M $NaBH_4$. However, real surface area ratio of the Cu/Ni/AuNi electrode to that of flat Au electrode calculated based on EIS results is about 2.0. Therefore it can be said that in addition to the increase in the surface area, a major part of the enhanced activity of the porous Cu/Ni/AuNi catalyst toward borohydride electrooxidation is due to the electrocatalytic activity resulting from improvement in the electronic properties of the catalyst.

3.4. Chronoamperometry and chronopotentiometry

Fig. 8A shows the chronoamperometric response of 0.02 M $NaBH_4$ in the case of a potential step from −0.8 to −0.1 V vs. SCE on both flat Au and Cu/Ni/AuNi electrodes. Fig. 8A shows that, for two samples, the potential-static currents decrease rapidly in the initial stage and then decay during the electrooxidation of $NaBH_4$. After 120 s, the Cu/Ni/AuNi electrode delivers higher current density (13 mA cm^{-2}) than the flat Au electrode (7 mA cm^{-2}). This result also confirmed that the Cu/Ni/AuNi electrode has a higher electrocatalytic activity and better stability than the flat Au electrode.

The number of electrons involved in the oxidation (n) on Cu/Ni/AuNi electrode can be determined by the use of the Cottrell equation [44]:

$$i = \frac{nFAC_0\sqrt{D_0}}{\sqrt{\pi t}} \quad (12)$$

where A is the active area of the work electrode, F is Faradaic constant, D_o is the diffusion coefficient and C_0 is bulk borohydride concentration. By application of Eq. (12), the $nD^{1/2}$ relation was calculated as 0.0136 cm $s^{-1/2}$. If the value of D_0 is 1.0×10^{-5} cm^2 s^{-1} [35,36], the total number of electrons (n) involved in the oxidation will be 4.3. The $nD^{1/2}$ relation and n value have been calculated by this method were approximately in agreement the CV measurements. The n value obtained indicates the direct oxidation of $NaBH_4$ is incomplete at peak a_2 and its oxidation product is oxidized at more positive potentials.

Fig. 8B compares the chronopotentiogram of flat Au and Cu/Ni/AuNi electrodes in 2 M NaOH + 0.02 M $NaBH_4$ solution. A current density of 5 mA cm^{-2} was applied to the electrodes for 120 s exposed to 2 M NaOH + 0.02 M $NaBH_4$ solution. It can be clearly seen from Fig. 8B that the polarization potential of the flat Au electrode gradually increases with time, and at the same transition time the Cu/Ni/AuNi electrode shows a much lower polarization potential than flat Au by about 0.20 V, suggesting that the Cu/Ni/AuNi can apparently reduce the electrochemical polarization of BH_4^- on electrooxidation process and improve electrocatalytic activities of BH_4^- oxidation. Therefore, it is potentially possible to obtain much higher power output on the Cu/Ni/AuNi anode. This is attributed to the structure of Cu/Ni/AuNi, namely, the porous and nanostructure is more favorable for mass transfer of liquid fuel and can improve the kinetics of $NaBH_4$ electrooxidation [45].

4. Conclusions

The present study reports on the successful synthesis of porous Cu/Ni/AuNi nanocatalyst by a simple galvanic replacement reaction of Cu/Ni/ZnNi in an alkaline gold solution. The electrooxidation of BH_4^- on a Cu/Ni/AuNi electrode has been systematically studied by CV, chronoamperometry, chronopotentiometry and EIS techniques. The results were compared with flat Au electrode in 2 M NaOH solution.

The SEM results showed that the Au nanoparticles in Cu/Ni/AuNi catalyst were highly dispersed and the alkaline leaching-galvanic replacement process produces a highly porous catalytic surface suitable for use in electrooxidation of borohydride.

The cyclic voltammetry experiment shows that current densities for borohydride oxidation on Cu/Ni/AuNi electrode (31 mA cm^{-2}) are greater than that observed for flat Au electrode (5.2 mA cm^{-2}) because the Cu/Ni/AuNi possesses smaller average size of the metal particles and improvement in the electronic properties of the catalyst. The EIS responses were found to be strongly dependent on electrode potentials. Also, the results of EIS measurement were consistent with the results of CVs and confirmed porosity of the Cu/Ni/AuNi electrode. The chronoamperometry, chronopotentiometry studies also confirmed high electrocatalytic activity and stability of Cu/Ni/AuNi catalyst for borohydride electrooxidation.

In general, all results show that the nanostructured Cu/Ni/AuNi electrode is a promising catalyst toward borohydride oxidation in alkaline media for fuel cell applications.

Acknowledgments

The authors would like to acknowledge the financial support of Renewable Energy Organization of Iran and the Office of Vice Chancellor in Charge of Research of University of Tabriz.

References

[1] B.C. Chan, R. Liu, K. Jambunathan, H. Zhang, G. Chen, T.E. Mallouk, E.S. Smotkin, Comparison of high-throughput electrochemical methods for testing direct methanol fuel cell anode electrocatalysts, J. Electrochem. Soc. 152 (2005) A594.
[2] B.K. Kho, B. Bae, M.A. Scibioh, J. Lee, H.Y. Ha, On the consequences of methanol crossover in passive air-breathing direct methanol fuel cells, J. Power Sources 142 (2005) 50.
[3] D. Chu, R. Jiang, Novel electrocatalysts for direct methanol fuel cells, Solid State Ionics 148 (2002) 591.
[4] E. Peled, T. Duvdevani, A. Aharon, A. Melman, New fuels as alternatives to methanol for direct oxidation fuel cells, Electrochem. Solid State Lett. 4 (2001) A38.
[5] C. Celik, F.G. Boyaci San, H.I. Sarac, Effects of operation conditions on direct borohydride fuel cell performance, J. Power Sources 185 (2008) 197.
[6] C. Celik, F.G. Boyaci San, H.I. Sarac, Influences of sodium borohydride concentration on direct borohydride fuel cell performance, J. Power Sources 195 (2010) 2599.
[7] X. Liu, L. Yi, X. Wang, J. Su, Y. Song, J. Liu, Graphene supported platinum nanoparticles as anode electrocatalyst for direct borohydride fuel cell, Int. J. Hydrogen Energy 37 (2012) 17984.
[8] I. Merino-Jiménez, C. Ponce de León, A.A. Shah, F.C. Walsh, Developments in direct borohydride fuel cells and remaining challenges, J. Power Sources 219 (2012) 339.
[9] Z.P. Li, B.H. Liu, K. Arai, K. Asaba, S. Suda, Evaluation of alkaline borohydride solutions as the fuel for fuel cell, J. Power Sources 126 (2004) 28.
[10] B.H. Liu, Z.P. Li, K. Arai, S. Suda, Performance improvement of a micro borohydride fuel cell operating at ambient conditions, Electrochim. Acta 50 (2005) 3719.
[11] N.A. Choudhury, R.K. Raman, S. Sampath, A.K. Shukla, An alkaline direct borohydride fuel cell with hydrogen peroxide as oxidant, J. Power Sources 143 (2005) 1.
[12] C. Ponce de Leon, F.C. Walsh, A. Rose, J.B. Lakeman, D.J. Browning, R.W. Reeve, A direct borohydride-acid peroxide fuel cell, J. Power Sources 164 (2007) 441.
[13] R.L. Pecsok, Polarographic studies on the oxidation and hydrolysis of sodium borohydride, J. Am. Chem. Soc. 75 (1953) 2862.
[14] M.H. Atwan, C.L.B. Macdonald, D.O. Northwood, E.L. Gyenge, Colloidal Au and Au-alloy catalysts for direct borohydride fuel cells: electrocatalysis and fuel cell performance, J. Power Sources 158 (2006) 36.
[15] J.H. Morris, H.J. Gysing, D. Reed, Electrochemistry of boron compounds, Chem. Rev. 85 (1985) 51.
[16] V. Baglio, A. Stassi, A. Di Blasi, C. D'Urso, V. Antonucci, A.S. Arico, Investigation of bimetallic Pt-M/C as DMFC cathode catalysts, Electrochim. Acta 53 (2007) 1360.
[17] M.B. Vukmirovic, J. Zhang, K. Sasaki, A.U. Nilekar, F. Uribe, M. Mavrikakis, R.R. Adzic, Platinum monolayer electrocatalysts for oxygen reduction, Electrochim. Acta 52 (2007) 2257.
[18] H.A. Gasteiger, N. Markovic, P.N. Ross Jr., E.J. Cairns, Methanol electrooxidation on well-characterized Pt–Ru alloys, J. Phys. Chem. 97 (1993) 12020.
[19] E. Antolini, J.R.C. Salgado, E.R. Gonzalez, The methanol oxidation reaction on platinum alloys with the first row transition metals: the case of Pt–Co and Pt–Ni alloy electrocatalysts for DMFCs: a short review, Appl. Catal. B: Environ. 63 (2006) 137.
[20] C. Ponce de Leon, F.C. Walsh, D. Pletcher, D.J. Browning, J.B. Lakeman, Direct borohydride fuel cells, J. Power Sources 155 (2006) 172.
[21] S.C. Amendola, P. Onnerud, M.T. Kelly, P.J. Petillo, S.L. Sharp-Goldman, M. Binder, A novel high power density borohydride-air cell, J. Power Sources 84 (1999) 130.
[22] R.X. Feng, H. Dong, Y.D. Wang, X.P. Ai, Y.L. Cao, H.X. Yang, A simple and high efficient direct borohydride fuel cell with MnO_2-catalyzed cathode, Electrochem. Commun. 7 (2005) 449.
[23] M.V. Mirkin, H. Yang, A.J. Bard, Borohydride oxidation at a gold electrode, J. Electrochem. Soc. 139 (1992) 2212.
[24] E. Gyenge, Electrooxidation of borohydride on platinum and gold electrodes: implications for direct borohydride fuel cell, Electrochim. Acta 49 (2004) 965.
[25] D.M.F. Santos, C.A.C. Sequeira, Determination of kinetic and diffusional parameters for sodium borohydride oxidation on gold electrodes, J. Electrochem. Soc. 156 (2009) F67.
[26] M.A. AbdelRahim, R.M. AbdelHameed, M.W. Khalil, Nickel as a catalyst for the electro-oxidation of methanol in alkaline medium, J. Power Sources 134 (2004) 160.
[27] G. Vértes, G. Horányi, Some problems of the kinetics of the oxidation of organic compounds at oxide-covered nickel electrodes, J. Electroanal. Chem. 52 (1974) 47.
[28] P.M. Robertson, On the oxidation of alcohols and amines at nickel oxide electrodes: mechanistic aspects, J. Electroanal. Chem. 111 (1980) 97.
[29] M.G. Hosseini, M. Abdolmaleki, S. Ashrafpoor, Preparation, characterization, and application of alkaline leached Ni/Zn–Ni binary coatings for electrooxidation of methanol in alkaline solution, J. Appl. Electrochem. 42 (2012) 153.
[30] M.G. Hosseini, M.M. Momeni, M. Faraji, Highly active nickel nanoparticles supported on TiO_2 nanotube electrodes for methanol electrooxidation, Electroanalysis 22 (2010) 2620.
[31] A. Aytaç, M. Gürbüz, A. Elif Sanli, Electrooxidation of hydrogen peroxide and sodium borohydride on Ni deposited carbon fiber electrode for alkaline fuel cells, Int. J. Hydrogen Energy 36 (2011) 10013.
[32] A.J. Bard, L.R. Faulkner, Electrochemical Methods: Fundamental and Applications, John Wiley & Sons, New York, 1980.
[33] E. Gileadi, E. Kirowa-Eisner, J. Penciner, Interfacial Electrochemistry, Addison-Wesley, London, 1975, pp. 373.
[34] D.M.F. Santos, C.A.C. Sequeira, Cyclic voltammetry investigation of borohydride oxidation at a gold electrode, Electrochim. Acta 55 (2010) 6775.
[35] K.L. Wang, J.T. Lu, L. Zhuang, Direct determination of diffusion coefficient for borohydride anions in alkaline solutions using chronoamperometry with spherical Au electrodes, J. Electroanal. Chem. 585 (2005) 191.
[36] G. Denuault, M.V. Mirkin, A.J. Bard, Direct determination of diffusion coefficients by chronoamperometry at microdisk electrodes, J. Electroanal. Chem. 308 (1991) 27.
[37] C. Hitz, A. Lasia, Experimental study and modeling of impedance of the HER on porous Ni electrodes, J. Electroanal. Chem. 500 (2001) 213.
[38] A. Lasia, Impedance of porous electrodes, J. Electroanal. Chem. 397 (1995) 27.
[39] L. Birry, A. Lasia, Studies of the hydrogen evolution reaction on Raney nickel–molybdenum electrodes, J. Appl. Electrochem. 34 (2004) 735.
[40] J. Kubisztal, A. Budniok, A. Lasia, Study of the hydrogen reaction on nickel-based composite coatings containing molybdenum powder, Int. J. Hydrogen Energy 32 (2007) 1211.
[41] S.S. Abdel-Rehim, K.F. Khaled, N.S. Abd-Elshafi, Electrochemical frequency modulation as a new technique for monitoring corrosion inhibition of iron in acid media by new thiourea derivative, Electrochim. Acta 51 (2006) 3269.
[42] L. Chen, A. Lasia, Study of the kinetics of hydrogen evolution reaction on nickel–zinc powder electrodes, J. Electrochem. Soc. 139 (1992) 3214.
[43] S. Trasatti, O.A. Petrii, Real surface area measurements in electrochemistry, Pure Appl. Chem. 63 (1991) 711.
[44] A.J. Bard, L.R. Faulkner, Electrochimie-Principes Méthodes et Applications, Masson, Paris, 1983.
[45] J.H. Kim, H.S. Kim, Y.M. Kang, M.S. Song, S. Rajendran, S.C. Han, D.H. Jung, J.Y. Lee, Carbon-supported and unsupported Pt anodes for direct borohydride liquid fuel cells, J. Electrochem. Soc. 151 (2004) A1039.